

Article

Integrating remote sensing and field investigation for lithological mapping of Per-Eonile to Neonile sequences west of Sohag city, Egypt: Impact on urban development

Bosy A. El-Haddad^{1,*}, Ahmed M. Youssef^{1,2,*}, Tawfiq M. Mahran¹, Abdel Hamed El-Sharter¹¹ Geology Department, Faculty of Science, Sohag University, Sohag 82524, Egypt² Geological Hazards Department, Geological Hazard Center, Saudi Geological Survey, Jeddah 21514, Saudi Arabia* **Corresponding authors:** Bosy A. El-Haddad, bosyelhaddad1987@gmail.com; Ahmed M. Youssef, amyoussef70@yahoo.com

CITATION

El-Haddad BA, Youssef AM, Mahran TM, El-Sharter AH. Integrating remote sensing and field investigation for lithological mapping of Per-Eonile to Neonile sequences west of Sohag city, Egypt: Impact on urban development. *Journal of Geography and Cartography*. 2024; 7(1): 6028. <https://doi.org/10.24294/jgc.v7i1.6028>

ARTICLE INFO

Received: 25 April 2024

Accepted: 8 May 2024

Available online: 23 May 2024

COPYRIGHT



Copyright © 2024 by author(s).

Journal of Geography and Cartography is published by EnPress Publisher, LLC. This work is licensed under the Creative Commons Attribution (CC BY) license.

<https://creativecommons.org/licenses/by/4.0/>

Abstract: In the domains of geological study, natural resource exploitation, geological hazards, sustainable development, and environmental management, lithological mapping holds significant importance. Conventional approaches to lithological mapping sometimes entail considerable effort and difficulties, especially in geographically isolated or inaccessible regions. Incorporating geological surveys and satellite data is a powerful approach that can be effectively employed for lithological mapping. During this process, contemporary RS-enhancing methodologies demonstrate a remarkable proficiency in identifying complex patterns and attributes within the data, hence facilitating the classification of diverse lithological entities. The primary objective of this study is to ascertain the lithological units present in the western section of the Sohag region. This objective will be achieved by integrating Landsat ETM⁺ satellite imagery and field observations. To achieve our objectives, we employed many methodologies, including the true and false color composition (FCC&TCC), the minimal noise fraction (MNF), principal component analysis (PCA), decoration stretch (DS), and independent component analysis (ICA). Our findings from the field investigation and the data presented offer compelling evidence that the distinct lithological units can be effectively distinguished. A recently introduced geology map has been incorporated within the research area. The sequence of formations depicted in this map is as follows: Thebes, Drunka, Katkut, Abu Retag, Issawia, Armant, Qena, Abbassia, and Dandara. Implementing this integrated technique enhances our comprehension of geological units and their impacts on urban development in the area. Based on the new geologic map of the study area, geologists can improve urban development in the regions by detecting building materials “aggregates”. This underscores the significance and potential of our research in the context of urban development.

Keywords: RS; lithological mapping; Landsat ETM⁺; Nile evolution; sustainable development

1. Introduction

Geological mapping is crucial in most geological studies, mineral exploration, geological hazard assessment, and environmental management [1]. It provides vital insights into the Earth’s crust’s distribution, composition, and geological history [2]. Accurate lithological maps offer a detailed understanding of different rock types’ distribution, properties, and characteristics within a study area. However, traditional methods of lithological mapping involve intensive fieldwork, which is time-consuming and challenging in inaccessible areas [3,4]. This is where remote sensing data proves valuable, as it can furnish detailed information across vast regions, particularly in semi-arid and arid areas [5]. Lithological mapping can be achieved

rapidly, cost-effectively, and accurately by amalgamating remote sensing and fieldwork [6]. This approach offers several advantages compared to other techniques, including integrating multiple data sources, which enhances the accuracy and comprehensiveness of lithological maps. Additionally, it enables the provision of up-to-date information on areas undergoing rapid changes due to anthropogenic factors while being capable of handling large amounts of data.

Various image-processing techniques have been developed in recent decades to improve, delineate, and classify geological characteristics, including alteration zones and tectonic lineaments [7]. Multiple studies have been conducted on the classification of lithologic units [8], and recent advancements in image-processing techniques in remote sensing have opened new possibilities for lithological mapping [9]. Advanced remote sensing enhancing processes can be used to recognize patterns and features in data and classify them into different lithological units. Integrating remote sensing and field investigation processes is faster, more efficient, and more accurate than the traditional “field survey” [10]. On the other hand, remote sensing techniques can process large amounts of data from various sources, such as multispectral and hyperspectral satellite imagery, field data, and geological and topographical maps [11]. This facilitates the integration of multiple data sources, thereby enhancing the precision of lithological maps.

Sustainable development of human society is closely related to geosciences by scientifically reviewing contributions made by geosciences to promote the geosciences to address the challenge faced [12]. It emphasizes the crucial role of geology in future urban planning, which significantly contributes to limiting conflicts, reducing risks, and lowering the costs of subsurface challenges [13]. Urban areas may tackle challenges by managing the subsurface based on geological knowledge and data. Geological maps play a significant role in urban development by providing the extensive data archives and cutting-edge expertise necessary for sustainable urban development [14].

The area under consideration represents a part of the Nile Valley. The lithostratigraphy of the sediments exposed in the study area has been studied by many authors [15–18]. Recently, Said [19] reviewed the earlier classifications of the Nile sediments and proposed new lithostratigraphic classifications in which the Nile sequence is classified from bottom to top into Madamud, Armant, Issawia, Qena, Abbassia, and Dandara formations. The various rock units at Sohag are composed of a sedimentary succession ranging in age from the Lower Eocene to the Quaternary [20].

The present work considers the nomenclature Said [21] gave for the Nile sediments. The detailed field study, the constructed geological maps and cross sections using satellite images (Landsat7 (ETM⁺)), and new remote sensing processing techniques have shown that these sediments exhibit significant lateral and vertical lithological variations. These characteristic features have yet to be illustrated among the different formations proposed by the earlier literature, enabling the authors to redefine the boundaries of some rock units proposed by Said [19] and to recognize new rock units not mentioned before in the stratigraphy of the Nile sediments. In addition to understanding the role of geology maps in urban sustainable development in the area.

2. Study area

The study area is located west of Sohag City. It includes the old floodplain and part of the western limestone plateau (**Figure 1a**). It is situated between the longitudes of 31°25' and 32°00' East and the latitudes of 26°00' and 26°35' North (**Figure 1b**), and it has an area of approximately 2164 km². To the east, it is surrounded by the recent Nile Valley floodplain. The highway that connects Cairo and Aswan passes through the middle of the study area. The area may be reached by many asphalt highways linking it to the cities. Several wadis also dissect the area. The area's elevation ranges from 63 m in the east to 393 m in the west.

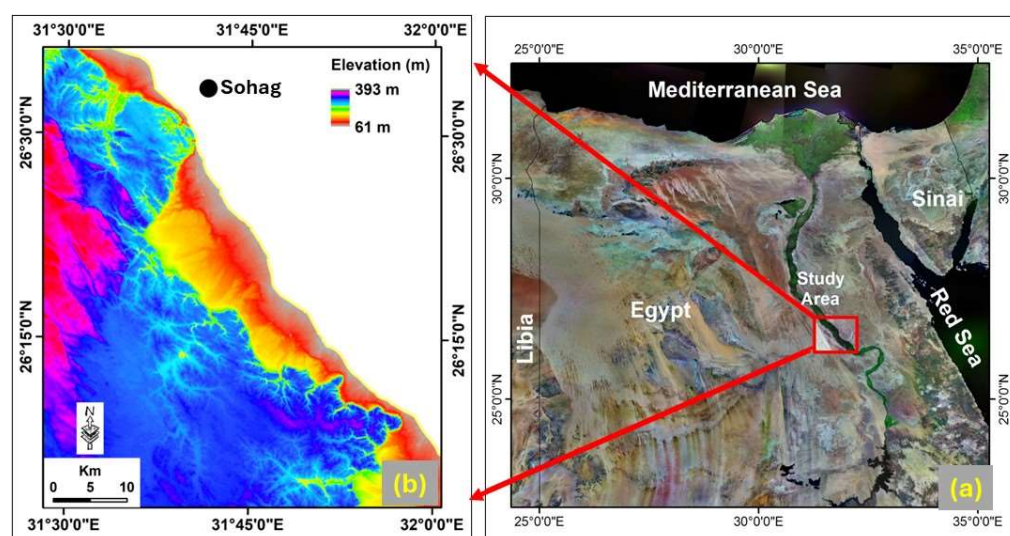


Figure 1. (a) Location map of the study area; (b) elevation map of the study area.

3. Data used and method

Remote sensing enables identifying, measuring, and analyzing various characteristics of target objects located on, above, or even below the earth's surface without direct contact between the sensors and the observed targets or events [2]. It allows for the extraction of information regarding the characteristics of objects by detecting and capturing the reflected or emitted energy, followed by the processing, analysis, and application of that acquired information [22]. Remote sensing data primarily consists of the reflected or emitted electromagnetic radiation from the targets. These data can be detected by a sensor usually mounted on airborne or spaceborne platforms. The application of remote sensing technology for lithological mapping has gained widespread application due to its ability to detect and differentiate surface characteristics that are not visible to the naked eye. Various remote sensing techniques are employed for lithological mapping, including hyperspectral imaging [1] and multispectral imaging [10,23]. Multispectral imaging involves collecting data in a few broad spectral bands with moderate spectral resolution and rapid coverage of large areas [24]. Its application in lithological mapping involves distinguishing between different lithological units by analyzing their spectral signatures. The limitation of remote sensing data can be overcome by integrating it with field investigation to improve the accuracy and efficiency of multispectral imaging.

In recent decades, Landsat satellites have provided valuable multispectral remote sensing datasets for various applications, including mapping rock types and mineral deposits [9]. The Landsat series includes several types, such as Landsat Thematic Mapper (TM), Enhanced Thematic Mapper Plus (ETM⁺), and Landsat Operational Land Imager (OLI). In the current study, Landsat-7 launched on 15 April 1999, carries the Enhanced Thematic Mapper Plus (ETM⁺) sensor, which was used. ETM⁺ offers seven spectral bands: Visible (B1, B2, B3), Near-Infrared (B4), and Short-Wave Infrared (B5, B7) with 30 m spatial resolution and a panchromatic band (B8) with 15 m spatial resolution. The sixth band (B6) is Thermal Infrared (with 60 m spatial resolution). The flowchart in **Figure 2** illustrates the method used in the current study. Various techniques were applied in the current research, including true and false color composites (TCC & FCC), principle component analysis (PCA), minimum noise fraction (MNF), decoration stretching (DS), and Independent Component Analysis (ICA). In addition, a field investigation was conducted to study the lithological framework. Various lithological sections were measured and acquired to verify the remote sensing results. Finally, evaluate the role of the geological mapping of the study area on urban development in the area.

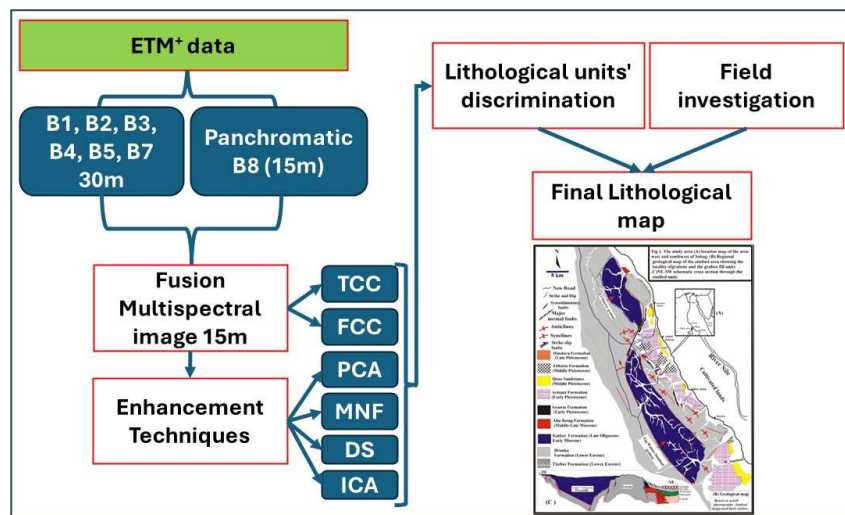


Figure 2. Flowchart showing the methodology of lithological unit mapping of the study area.

4. Results and discussion

4.1. Remote sensing analysis

This study applied a true-color composite (bands 321 in RGB) (**Figure 3a**). The results indicated that it was not helpful for lithological analysis. The image only offers a little information, except for discriminating between the bedrock units (limestone) and the fan deposits (sediments) under the scarp. In addition, a false-color composite (bands 742) has been produced (**Figure 3b**). It was found that the false color is somehow helpful for lithological analysis. In this image, aggregate deposits appear with a dark to light brown color, vegetation in green, and other materials in a light color. However, this composite did not clearly distinguish between different types of aggregate materials and the surrounding deposits.

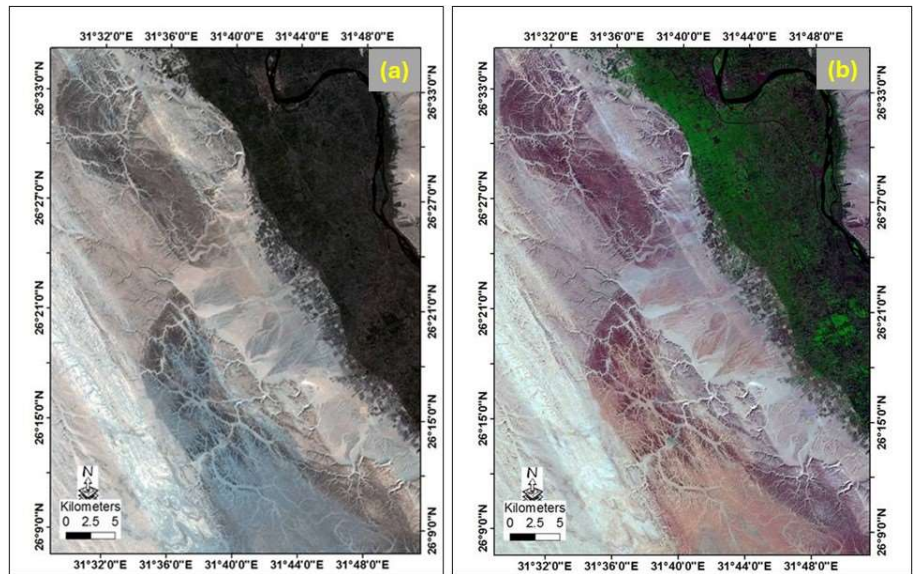


Figure 3. (a) a true color composite of Landsat ETM⁺ bands 321 in (RGB); (b) a false color composite bands 742 in (RGB).

Note: The Katkut Formation appears to be distributed in brick and brown colors.

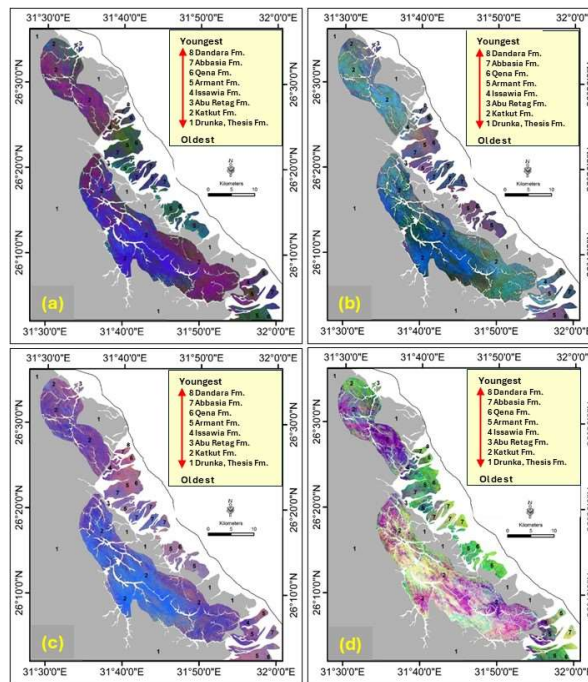


Figure 4. (a) PC image bands 124 in RGB; (b) MNF image 531 in RGB; (c) DS image 321 in RGB; (d) ICA image 561 in RGB. Drunka, Katkut, Abu Retag, Issawia, Armant, Qena, and Abbassia formations take numbers 1 to 7 in the image, respectively.

Several enhancing remote sensing processes were applied to bands 1, 2, 3, 4, 5, and 7 of the ETM⁺ image. 1) Principal component analysis (PCA) was applied, as shown in **Figure 4a**. The best PC combination was band 124 in RGB, respectively. 2) The minimum noise fraction (MNF) technique was applied, as shown in **Figure 4b**. Results show that the MNF band 531 in RGB provides the best discrimination between various rock units. 3) The decorrelation stretch (DS) was applied to the selected band

triplet (321 in RGB) (**Figure 4c**). Results show that this DS combination succeeded in differentiating the different rock units from each other and the surrounding materials. 4) The independent component analysis (ICA) was applied to the study area's image data to enhance the image's spectral variability. **Figure 4d** shows the ICA band 156 in RGB. This combination from ICA differentiated the different rock units in the study area. These four advanced techniques (PCA, MNF, DS, and ICA) successfully distinguished the different sedimentary rock units from each other and the surrounding materials. These units include Drunka (1), Katkut (2), Abu Retag (3), Issawia (4), Armant (5), Qena (6), and Abbassia (7) formations (**Figure 4a–d**). Based on the analysis of these methods, they are instrumental in discriminating between different exposed rock units.

4.2. Field investigation and lithological formations

Generally, these sediments are grouped into three primary lithostratigraphic sequences: the Lower Eocene limestone sequence, the Late Oligocene-Late Miocene sequence (Pre-Eonile–Eonile), and the Pliocene-Quaternary sequence (Paleonile-Neonile). Each sequence is distinct in lithology and stratigraphic relationships and is limited by apparent structural discordance. **Figure 5** summarizes the proposed lithostratigraphy of the rock units of the study area.

Age	Rock units	Nile Stages
Late-Pleistocene	Dandara Formation	Neonile
Middle-Pleistocene	Abbassia Formation	Prenile
	Qena Formation	
Early-Pleistocene	Armant Fm Issawia Fm	Protonile (Desert)
Middle-Late Miocene	Abu Retag Formation	Eonile
Late Oligocene-Early Miocene	Katkut Fm	Pre-Eonile
Early Eocene	Drunka Fm	Early Eocene
	Thebes Formation	

Figure 5. Chronostratigraphic summary chart of late Oligocene-Pleistocene, sequences of the Pre-Eonile—Neonile stages of the Nile evolution at the west Sohag area.

4.2.1. The lower Eocene limestone sequence

Lower Eocene limestone plateaus border the study area's Nile Valley. Due to lithology and faunal content variations, this sequence is divided into two rock units: the Thebes Formation at the base and the Drunka Formation at the top.

The Thebes Formation: This formation represents the Lower Eocene limestone of the Nile Valley. Thebes Formation has a local distribution in the area west of Sohag. Lithologically, the Thebes Formation is characterized by 30 meters of laminated limestone with flint bands west of El-Kawamil village, where it conformably underlies the Drunka Formation (**Figure 6a**).

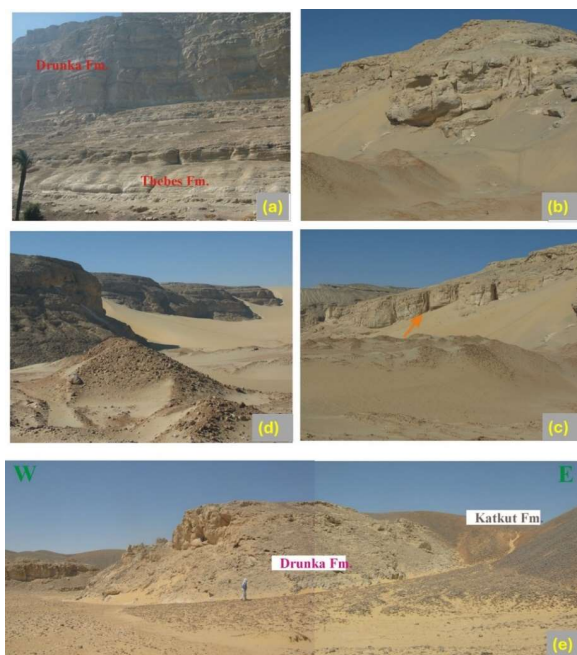


Figure 6. Field photographs showing: **(a)** the Drunka Fm. overlies the Thebes Fm.; **(b)** the massive and thick-bedded nature of the Drunka Fm.; **(c)** a tilted block of the Drunka Fm. The arrow points to fractures affected by the west-dipping fault block; **(d)** reentrant features due to the intersections of NW and ENE fault segments; **(e)** E-W oriented panoramas showing conglomerates of Katkut Fm.

The Drunka Formation: The Drunka Formation covers more than 90% of the area around Sohag. It overlies the Thebes Formation and is easily differentiated from it by its snow-white color and massive bedding (**Figure 6b**). The lower part of the Drunka Formation (~30 m) is composed of laminated limestone with chert bands interbedded with bioturbated hard massive limestone, including large, silicified limestone concretions (up to 1.2 m in diameter). The upper part (up to 100 m) comprises greyish-white, massive, bedded bioturbated limestone enriched with echinoderms, mollusks, large foraminifera, and calcareous algae. The field view shows the Drunka Formation affected by faults and reentrants due to the intersections of NW and ENE fault segments (**Figure 6c,d**). In addition, conglomerate deposits of the Katkut Formation are resting unconformably upon the E-dipping Eocene fault block, where the conglomerates are trapped west of blocks in some places (**Figure 6e**).

4.2.2. The Late Oligocene—Late Miocene sequence

4.2.2.1. The Katkut formation

Many authors first introduced the name Katkut Formation to the post-Eocene stratigraphy west of the Nile Valley [25,26]. It comprises all the coarse clastic sequences that unconformably overlie the Early Eocene sequence. In the current work, we use the name Katkut Formation to describe all coarse clastic sediments, which are entirely restricted to the filling of the NW grabens formed in the Early Eocene sequence along the Nile Valley western margin (**Figure 7a**). The type section for the Katkut Formation is located on the southern flank of Wadi El Yatim, where it measures more than 60 m thick. The base of this formation is not exposed to the surface. Considering the analysis of the sedimentary record, we have divided the Katkut

Formation into three unconformably bounded units; their boundaries correspond to changes in depositional and erosional processes (**Figure 7b,c**). Unit (1) comprises more than 15 m of conglomerates and conglomeratic sandstones. Some channel-like bodies are observed, and most sequences are fining upwards. The western margin of this unit is truncated by an angular unconformity against which coarse slope deposits have accumulated. Unit (2) is formed by 5 to 40 m thick cross-bedded sandstones. The remaining section is composed of mottled, reddish-brown siltstone and claystone. The top part of this unit includes terrigenous paleosol and calcrete nodules. The base of unit (3) is 20 m thick of tabular cross-bedded conglomeratic sandstones. The overlying section (5 to 20 m thick) comprises conglomerates and conglomeratic sandstones of varying proportions of extrabasinal material (mainly chert). In most cases, the beds display an upward-coarsening.

4.2.2.2. The Abu Retag formation

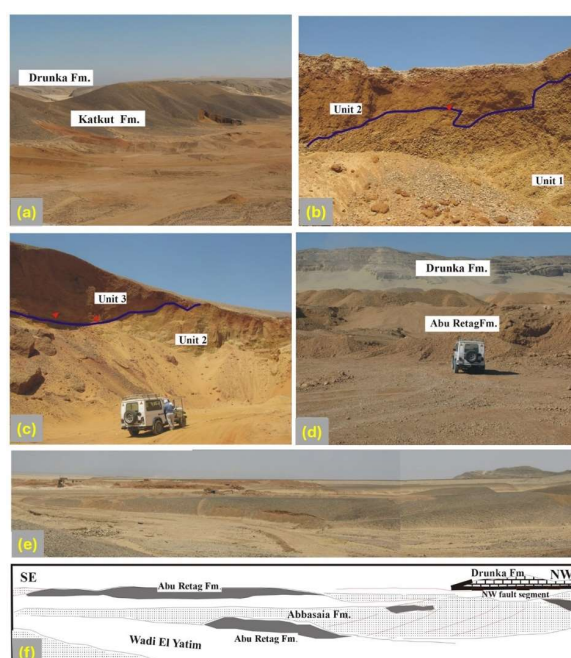


Figure 7. Field photographs showing (a) the Katkut Fm. filling NW-trending Graben; (b) Unit (2) unconformably overlying Unit (1) of Katkut Fm.; (c) Unit (3) unconformably overlying Unit (2); (d) the Eocene coarse clastics (Abu Retag Fm.) occurring in “Wadi Abu Retag”; (e) NW-SE panorama view; (f) line drawing of Abu Retag Fm. (gray color) unconformably overlying by Pre-Nile Abbasia Fm.

The formal name Abu Retag Formation has been newly introduced to the local stratigraphy of the Nile sediments by Mahran et al. [27] to describe the mottled reddish brown coarse clastic sediments that predominantly crop out along the lower slopes of the western Eocene limestone scarps (**Figure 7d**). It is well developed in the hanging wall of the NW, N, and NE fault segments, where the Eocene plateau is intensely faulted (**Figure 7e**). The Abu Retag Formation forms the first stage of fluvial sedimentation within the Nile basin fill. The line drawing of the view south of Wadi El Yatim shows the Abu Retag Formation (gray color) extending east of the Drunka Formation and unconformably overlying the Pre-Nile Abbasia Formation. Foreset dips

of Abbassia conglomerates indicate an eastward progradation direction (**Figure 7f**). Some of the Abbassia Formation is trapped within depressions west of the Abu Retag deposits. Locally, the Abu Retag deposits unconformably overlie the tilted carbonate blocks of the Drunka Formation. The thickest section of the Abu Retag Formation was measured at the northern flank of Wadi Abu Retag, where exposures occur in three closely spaced sections in boreholes. The most complete of these totals is about 50 m in thickness. These sediments comprise a wide range of clast sizes and extrabasinal (silicified and biogenic limestones, cherts, and sandstones). Basement clasts are also present and localized in the upper part of the conglomerate section. Bedding varies from massive to crudely stratified to trough cross-bedding. Most of the sequence exhibits a coarsening-upward depositional trend. Individual beds are commonly lenticular in shape and have irregular bases. Paleosol horizons and desiccation cracks are common in these sediments.

4.2.3. The Pliocene—Quaternary sequence

The Pliocene-Quaternary sequence in the study area (west of Sohag city), belonging to the Paleocene-Pliocene stages, forms the Nile terraces between the cultivated flood plains and western Eocene limestone cliffs. This sequence is classified into five lithostratigraphic units: Armant, Issawia, Qena, Abbassia, and Dandara formations.

4.2.3.1. The Issawia formation

Said [28] used “Issawia Formation” to describe a succession of massive rubble breccias topped by characteristic hard red breccias. Careful examination of aerial photographs, Landsat-7 ETM⁺ images, and facies analysis indicate that both Issawia and Armant formations are laterally interfingering; hence, the sediments of the two units were contemporaneously deposited. Sediments of the Issawia Formation crop out along the margins of the Eocene escarpment. The type section is measured south of Wadi El-Kiman, where it attains its maximum thickness of up to 30 m. It is subdivided into three units, separated by paleosol horizons. The lower unit comprises breccia clasts ranging from 0.3 to 3 m in diameter. The middle unit is dominated by crudely bedded breccias of different sizes. The clasts tend to decrease in size westward. The upper unit has a wedge-like geometry and is composed of thick-bedded conglomerates. Laterally, the conglomerates intercalate with calcrete and palustrine beds. Generally, the sequence of the Issawia Formation is terminated by hard red breccias reaching about 10 m in thickness. At Wadi El Yatim, west of Sohag, the Issawia Formation crops out, plastering the foot of the western scarp. It is represented by inclined beds of hard red breccias (up to 15 m thick, **Figure 8a,b**).

This facies association consists of aggradational stacked crudely bedded breccias displaying aggradation upper contact and is often interbedded with calcrete and palustrine limestone. The beds are mostly disorganized and occasionally inversely graded. Clasts of this breccia are monomictic in origin and are mostly derived from the Drunka Formation. Clasts are mostly angular or subangular. Boulder-size clasts are common (maximum 1.5 m on the long axis). Matrix consists mainly of fine-grained silt and sand, often argillaceous, and angular carbonate clasts. The top part is hard and cemented by ferruginous lamellar calcrete crusts. The predominance of crudely bedded breccia in steeply inclined contact with Eocene limestone indicates a localized

origin of sediment and a short transport distance. This local provenance, together with the angularity and monomictic composition, suggests sediment deposited as colluvial debris generated from the fractured bedrock on a steep-gradient slope. The extremely poor sorting and the local inverse grade of some breccia beds, as well as the disorganized fabric of clasts, are indicative of debris flow deposition.

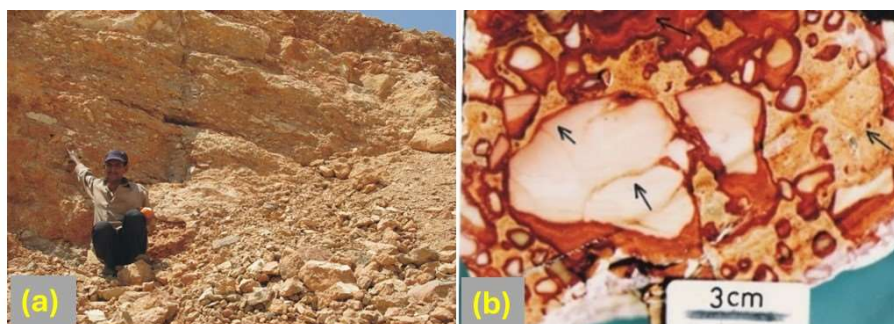


Figure 8. Field view showing the Issawia Formation. (Occurs at the footslope of the Eocene escarpment). **(a)** Red breccia cemented by ferruginous calcrete crusts; **(b)** close-up view of inclined crudely bedded breccias of different sizes.

4.2.3.2. The Armant formation

The name Armant Formation was first introduced into the stratigraphy of the Nile sediments by Said [15,28] to describe the fine-grained clastic beds alternating with bedded travertine carbonates. In the study area, the Armant Formation attains lateral lithological variations. West of Sohag, the Armant Formation is predominantly carbonates and tufas (averaging 10 to 20 m thick). Locally at Wadi El-Yatim, this formation unconformably overlies the Abu Retag Formation and underlies the Abbassia Formation (**Figure 9**). The temporal and spatial distribution of the sediments of the Armant Formation led to the recognition of two major lithofacies associations, as follows:

1) The peripheral facies associations occupying the lake's eastern margin. Siliciclastics, tufa, and associated carbonates dominate them. It is subdivided into three main facies: a) Fluvial channel facies, which consist of tabular cross-bedded medium- to coarse-grained sandstones indicating a northwesterly trending paleocurrent direction. This grades upward into laminated fine sandstone intercalated with siltstone and claystone. This sequence is terminated by massive conglomerates (up to 4 m thick) that interfingered laterally with tufas and palustrine limestone; b) Oncolytic facies, which consist of oncolites of variable size and shape. Three groups of oncolites are distinguished based on the lengths of the long axis: small (about 10 cm), large (10–25 cm), and giant oncolites (30 cm up to 1 m long). The small and large oncolites occur as lenticular bodies up to 50 cm thick, interfingering and directly overlying the conglomerate beds. Their nuclei consist of carbonate fragments. The thickness of the coatings ranges from a few millimeters up to 2 cm, and they are symmetrical or asymmetrical. The giant oncolites occur as ovoid shapes, from 40 cm to at least 1 m long, and in some cases, they have cylindrical shapes, resulting from microbialite-coated tree trunks and large stems. Giant oncolites are flat-laminate and undulatory, and the laminae tend to be continuous. Occasionally, the oncolites include

irregular pores and cavities filled with spar calcite; and c) Tufa facies, which are localized in the eastern margin of the lake. It is composed of boundstones, rudstones of calcite-coated phytoclasts, and in situ stems. Phytoclasts and intraclasts mainly constitute lenticular layers up to 3 m thick, interbedded near the base with ochre mudstones.

2) The second facies is the central lacustrine—palustrine facies associations. The strata that comprise the central lake basin can be characterized as two distinct lithofacies: the lacustrine and the palustrine carbonate facies. a) The lacustrine facies predominate in the southern outcrops of the entrance of Wadi Tag Waber and Wadi El Dukhan, and are represented by three distinct surfaces: a1) Micritic limestone, which is represented by tabular beds (1–1.5 m thick). Most beds have a mottled appearance, varying from gray to reddish yellow. In some places, the beds contain curved to straight veins filled with sparry calcite and siltstones. Subvertical root traces commonly extend from the upper contact of the beds and taper downward; a2) Ostracodal limestone overlies the micritic limestones. It is 2 m thick. The ostracods are mainly hosted by micritic wack stones and packstones, in which calcite spars fill some ostracod shells. Clastic grains are represented by quartz and carbonates and have an iron oxide coating. Locally, cracks, pores, and cavities are encountered, and they are filled with coarse calcite. a3) Intraclastic limestone, which contains grey angular to subangular clasts up to 5 cm in diameter that are mixed and not related to the underlying substrate. The limestone comprises clasts of varied composition: nodular micrites, carbonates, laminar, and brecciated limestones. The clasts are dispersed within a gray-yellow marly matrix. These intraclasts decrease down to silt size. b) The palustrine facies occupy the most abundant facies in the central lake basin. Two surfaces may be broadly recognized: limestone with irregular desiccation and root bioturbation; and nodular and brecciated limestones: b1) Limestone with irregular desiccation and root bioturbation is clastic free, and alternates with nodular and brecciated limestones. The interbeds have sharp lower and upper boundaries. This surface consists of micritic and microsparite with poorly preserved gastropod shells. Their thickness varies from 50 cm to 1 m. The desiccation cracks are well-pronounced at the tops of the beds and are recognized in thin sections as large and elongate cavities filled by intraclasts, quartz, and later sparry calcite cement; b2) Nodular and brecciated limestone is crudely bedded brownish yellow limestone and averages 1.5–3 m in thickness. The limestone clasts are micritic to microsparitic calcite and display a distinctive nodular structure and in-situ brecciation associated with red mottling. The nodular limestone beds display extensive vertical root traces up to 20 cm long.

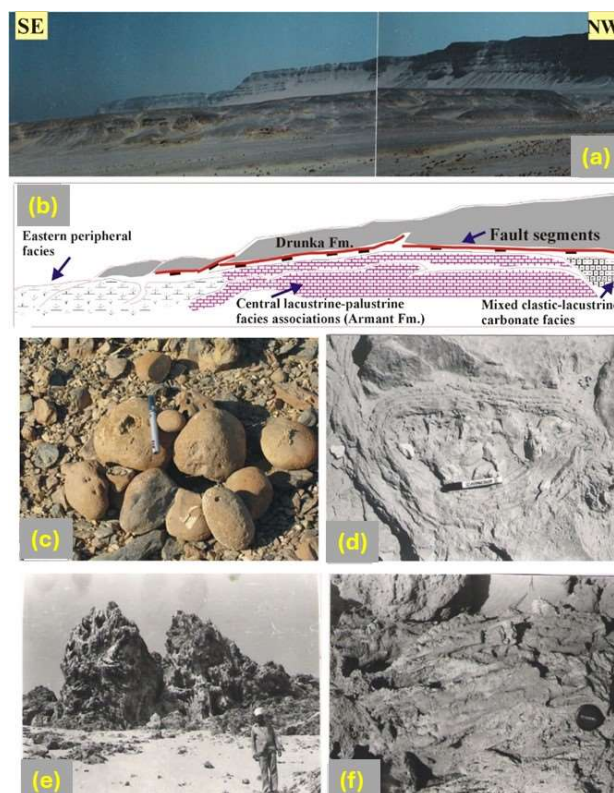


Figure 9. (a,b) Panorama and line drawing of view looking southeast along Wadi Tag Wabar showing the lateral facies association of Armant Formation; (c,d) close-up view of small and large oncolites, peripheral facies associations; (e) field view of tufa mounds, boundstones, and rudstones, tufa deposits facies; (f) a photograph of columnar tufa and large stems.

4.2.3.3. The Qena formation

Said [28] used the name Qena Formation to describe a thick succession of gravel-sand associations near the Qena area. The Qena Formation exhibits low-topographic hills with rounded surfaces and low scarps extending in the NW-SE direction near the cultivated land in the study area. West of Sohag City, many quarries are used to exploit the Qena Formation for construction purposes. A measured section at one of these quarries showed that the exposed section of the Qena Formation started at the base with cycles of cross-bedded coarse-grained sandstones, followed upwards by laminated and cross-laminated fine sandstones and siltstones.

The exposed 10 to 24 m thick Qena Formation west of Sohag is conglomeritic sandstone and sandstones. Three main surfaces are associated with the Qena Formation, mainly related to the fluvial in-channel process. They include 1) Facies (A) consisting of medium- to coarse-grained planar cross-bedded sandstones. This facies represents 50% of the total succession and consists of medium- to coarse-grained, poorly sorted quartz to feldspathic sandstones arranged into tabular sets, which are characterized internally by planar-cross bedding displaying a fining-upward trend. They show a unidirectional paleocurrent direction to the N and NW. Both high-angle (25°) and low-angle (10° – 15°) planar cross-bedding occur in these facies. Facies A is interpreted to form by the migration of straight-crested channel bars [29] deposited under conditions of a lower flow regime. The deposition of low-angle cross-bedding

within large-scale cross-bedding sets of these facies indicates that these large sets are a product of bar migration [30]. 2) Facies (B) are represented by ripple cross-laminated sandstones. This facies represents 20% of the total succession, overlies the planar cross-bedded sandstones, and consists of fine-to coarse-grained sandstones that are generally well sorted. It has a wedge-like geometry that pinches out laterally and contains asymmetrical ripple marks and small-scale sets of the trough and planar cross-stratification, load casts, and convolute beddings. Facies B represents slow sedimentation within largely inactive channels as fill deposits. The presence of asymmetrical current ripples and cross laminations indicates deposition by alternating subaqueous fractions and suspension processes in areas between bars or in overbank areas [31]. 3) Facies (C) are represented by flat-bedded sandstone and siltstone. This facies represents 10% of the total succession and consists of fine-to-medium-grained horizontally laminated sandstone. Weathered surfaces are a light-dark brown. Texturally, the sandstone is mostly subangular to subrounded, poorly sorted, and has intercalations of mica. Exposure evidence in these facies includes desiccation, calcrete nodules, and bioturbations. Facies (C) accumulate as planar beds under either an upper or low flow regime [32]. The thin, sheet-like geometry and fine-grained nature of the lithology suggest deposition as sand sheets or in-channel deposits during flood events' waning stages [33].

4.2.3.4. The Abbassia formation

The Abbassia Formation was first proposed by Said [15,28] to describe the gravel sequence overlying the Qena Sands. In the studied area, the Abbassia Formation occurs on the western bank of the River Nile. It can be easily distinguished in the field by its yellowish-grey to greyish-white coarse terrigenous clasts, which reach their maximum thickness in areas facing the major wadis draining the Eocene plateaus. West of Sohag, the Abbassia Formation is represented by a 10 m thick, unconformably overlying Armant Formation (e.g., Wadi El-Yatim, Wadi Dukhan, **Figure 5e**). Locally, these sediments are trapped in low-topographic areas west of the Armant and Abu Retag formations and are dominated by progradational conglomerates that laterally interfinger with sandstones and siltstones.

These sediments construct an alluvial fan of radiating distributary channels that nearly spread eastward and southeastward towards the Nile axis. Two main surfaces are recognized, the proximal alluvial fan and the alluvial plain: 1) The proximal alluvial fan crops out close to the Eocene escarpment and unconformably overlies the Abu Retag Formation. It is 3 m thick and consists of red, ochre, and grain-supported conglomerates. The gravels are arranged in progradational coarsening upwards. They are poorly sorted and immature. The gravels consist of Eocene carbonates (70%), cherts, and quartz (25%). These sediments were deposited by debris flow-dominated alluvial fans during high-energy episodic flows of flash floods. Paleocurrents measured on conglomerates and their textural changes indicate an eastward-down valley spreading. The clast composition suggests the local derivation of the source rocks. 2) The Alluvial plain is represented by vertical stacking fining-upward fluvial channel cycles. The bottom surface is erosive and irregular, cutting into the underlying one. Paleocurrent measurements from imbricated clasts and axis channel deposits indicate easterly and northeasterly trending transport. This sequence is terminated by

medium-to-fine-grained reddish-brown sandstones displaying a sheet-like geometry. These surfaces represent deposition in the middle to distal zones of the fluvial fan, where fluvial channels developed. The vertical stacking channel fills are interpreted as low-sinuosity fluvial channel deposits. Sheet floods in fluvial fans' more distal terminal areas formed sheet-like sandstone beds.

4.2.3.5. The Dandara formation

The name Dandara Formation was first proposed by Said [28] to describe the silt and fine sand section west of Dandara. In the study area, the Dandara Formation is generally closer to the cultivated land and is represented by sand and silt intercalations along the eastern bank of the Nile. West of Sohag, the Dandara Formation forms small hills composed of 5 m thick sand and silt intercalations with lenses of hard sandstones. The facies association can be divided into two main vertical surfaces: (i) 1 to 4 m thick packages composed entirely of massive to flat laminated mudstone with calcrete nodules. (ii) 2 m thick, coarsening-upward beds, composed of massive mudstones at their base, locally displaying mud cracks, overlain by fine sandstones with cross laminations. Massive and laminated mudstone is interpreted to represent overbank deposits accumulated through the setting of the suspended load within flooded areas [31]. The presence of mudcracks indicates ephemeral and subarid exposures. The coarsening-upward cycles are interpreted to represent shallow-lake marginal deposits formed due to the deceleration of streams as they enter water bodies.

5. Discussion

5.1. Age relations of the Late Oligocene—Late Miocene sequence

Due to the absence of marine fauna in such continental sediments, the authors assigned the strata of the Katkut Formation to the late Oligocene—early Miocene age based on the following: i) The NW-trending faults forming grabens, in which the sediments of the Katkut formation were deposited, clearly deform the Eocene limestone; hence, these grabens-fill sediments must be younger than the Eocene age. ii) The conglomerates of the Katkut Formation have a very close resemblance in composition with that of the known Late Oligocene conglomerates of Egypt through the correlation with other and similar lithologic units in nearby areas. These gravels are analogous to the Late Oligocene Nakheil Formation on the eastern side of the Red Sea Mountains, as described by Akkad and Dardir [34] and Mahran [35]. The later sediments are also composed of limestones and cherts and devoid of Precambrian basement pebbles. These deposits' rare granitic and volcanic rocks prove that the Precambrian Red Sea Mountains were not exposed during the early rift phase, which started during the Late Eocene—Early Oligocene.

The presence of basement pebbles in the Abu Retag Formation indicates that the basement in the Western Red Sea Mountains was exposed later in the Late Miocene than in the Eastern Red Sea Mountains (lower Miocene) and probably extended back to the Middle Miocene, especially since it is known that the valley of the Nile is considered as old as the Miocene [28]. Furthermore, the establishment of the Eonile stage of Said [28] during the Late Miocene time, as well as the stratigraphic position of the Abu Retag Formation by the interfingering with the upper parts of the Eonile

fine siliciclastic of the Nile Canyon of Said [28] during the Late Miocene, all give indications that the age of the Abu Retag Formation ranges from Middle to Late Miocene time.

5.2. Age relations of the Pliocene—Quaternary sequence

Said [28] gave the Pliocene age for the fine siliciclastics of the Madamud Formation. The Issawia and Armant formations unconformably overly channelized the Qena and Abbassia formations and are underlain by the Pliocene Madamud Formation. Hence, a post-Pliocene age is more likely. Thus, the authors propose that the age of the Issawia and Armant formations is early Pleistocene and is equivalent to the pluvial sediments of the Early Quaternary of Said [21].

The Locus of the Prenile system (Qena and Abbassia formations) as a separate terrace extending to the west of Early Pleistocene Protonile sediments (Issawia and Armant formations) indicates the Prenile system excavated its channel to the west of the Protonile after the later had ceased to flow. These formations are probably younger and could be considered Middle Pleistocene. Furthermore, most of the conglomerate clasts are either granites or gneisses, and their source is suggested to be the Precambrian basement rocks. Hence, it is most likely that the supply of these sediments began before its connection with sources outside of Egypt, which was established in the Late Pleistocene [21,36,37]. This indicates that the sediments of the Qena and Abbassia formations were deposited in the Middle Pleistocene. The interfingering Dandara and El Gir formations are dated to late Pleistocene age, based on the appearance of the Ethiopian mineral suite that was extracted from the Ethiopian highlands during the Late Pleistocene [17,21,28].

5.3. New geologic map of the west Sohag area

In the current research, Landsat ETM⁺, 15 m resolution, covers the study area and was used to map various lithological units. Environment for Visualizing Images (ENVI 5.5) software was used for data analysis and interpretation. Several image enhancement techniques have been applied to enhance the spectral differences between rock units. These techniques begin with True and False Color Composites (TCC&FCC), Principal Component Analysis (PCA), Minimum Noise Fraction (MNF), Decorrelation Stretching (DS), and Independent Component Analysis (ICA). The data was validated with extensive field investigation to identify these rock units, their contacts, and facies. Finally, the authors compiled the results, and a new lithologic map was prepared (**Figure 10**). The sediments belonging to the area west of Sohag are exhibited by two primary lithostratigraphic sequences (**Figure 11**). The older sequence belongs to the Late Oligocene-Late Miocene. It comprises dominantly coarse siliciclastic sequences deposited in low-topographic grabens and hangingwall fault segments (e.g., Katkut and Abu Retag formations). The younger sequence is of Plio-Pleistocene age and consists of mixed siliciclastics—carbonates and sandstones deposited in reentrants on the western side of the Nile basin (e.g., Issawia, Armant, Qena, Abbassia, and Dandara formations, **Figure 11**).

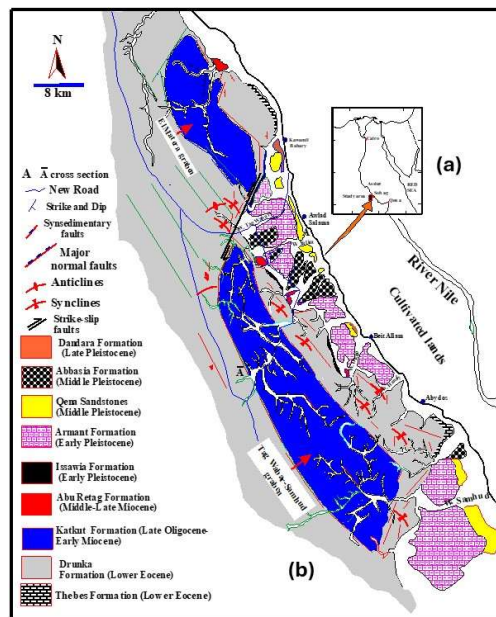


Figure 10. The study area. (a) A location map of the area west and southwest of Sohag; (b) a regional geological map of the study area showing the locality of grabens and the graben fill units.

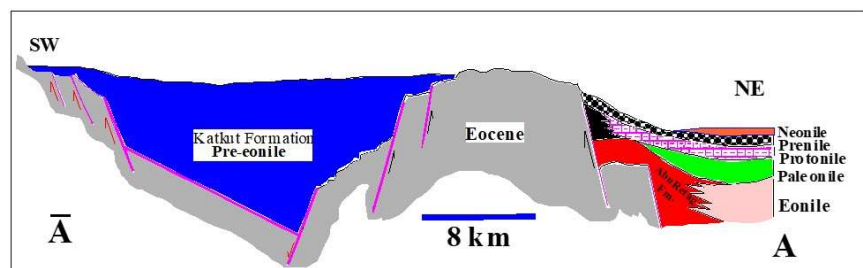


Figure 11. SW-NE cross section (A-A) showing the two main lithostratigraphic units of Pre-Eonile-Neonile sediments west of the Sohag area.

5.4. Geological mapping and urban development in the area

With time, there has been an increase in urban development operations being carried out in low desert zones (west Sohag desert areas). These operations have encompassed regions that have been an essential supply of natural resources, particularly aggregates. As a consequence, there is a diminished availability of these materials in the low desert zone [38]. Numerous projects have been underway throughout Egypt's regions, including substantial transportation initiatives, industrial zones, land reclamation, and urban activities since the 1980s. As a result of these recent construction operations, the vast majority of the quarries have been set aside and have yet to be utilized. This leads to the exploitation of aggregates produced in places that are entirely unsuitable for various purposes, particularly urban development.

The geologic map strives to understand the geological unit distributions, their composition, and their structures. Within the past few decades, geographic information systems (GIS) have begun to change aspects of geologic mapping by providing software tools that permit the geometry and characteristics of rock bodies and other

geologic features to be digitally stored, displayed, queried, and analyzed in conjunction with a seemingly infinite variety of different data types. Accordingly, GIS dramatically facilitates the analysis and, as a result, offers geologists the opportunity to provide information in map form that is easily interpreted and used by nongeologists (e.g., land use planners and decision-makers). Geologic mapping is a highly interpretive, scientific process that can also be used for assessing environmental issues (e.g., location of landfills), predicting various geologic hazards (problematic soils), industrial activities (aggregate accumulations), and, finally, education activities. These maps will have good benefit-cost analyses to reduce uncertainty for future projects. In the current study, and for urban development, the geologic map offers an essential location for new aggregate resources that could be used as construction materials (e.g., Katkut and Abu Retag formations). These materials are very close to urban areas, so the transportation cost is minimal.

6. Conclusion

Remote sensing is a commonly used tool in earth science, particularly for studying geological issues, such as lithological mapping. Remote sensing has garnered significant interest owing to its capacity to mitigate the expenses associated with field mapping, surmount challenges related to accessing specific locations, and identify regions exhibiting elevated levels of mineralization and alteration. The data acquired using the conventional methodology were derived from field surveys. The collected data exhibit notable limitations that impact the goals of the present investigation. The combination of Remote Sensing (RS) and Field Survey offers significant potential for cost reduction in field mapping and overcoming constraints related to field access. The lithological units and facies of the research region were accurately delineated through satellite image processing and field data collection. The PCA, MNF, DS, and ICA techniques have shown significant efficacy in distinguishing geological characteristics. The field study conducted as part of this work facilitated the comparison and evaluation of the effectiveness of remote sensing data in the cartographic representation of sedimentary units. Precise outcomes are obtained using RS methodologies, such as color compositions, MNF, PCA, ICA, and DS. The combination of these bands holds significant importance in identifying lithological formations. Using PC1, PC2, and PC3, a more optimal combination of the color composite was achieved, leading to enhanced results in the cartographic representation of the geological units encompassed within the designated research area. Moreover, the most notable maps were meticulously crafted with meticulous attention to detail. The current geological map of the region is scaled at a ratio of 1/250,000, resulting in poor spatial resolution. However, applying satellite imagery for lithology mapping provides higher precision, characterized by a high spatial resolution. In summary, satellite imagery for lithology mapping provides a notable level of spatial resolution. Despite the advantages above, it is imperative to remember that RS methodologies cannot detect minuscule entities, necessitating their enhancement. These approaches are highly efficient and accurate for comprehending the geological features of a particular site. Using remote sensing technology enables the acquisition of a wide range of data over extensive geographical regions. The current step of the procedure

involves the introduction of two new lithological units, namely the Katkut and Abu Retag formations. These approaches are highly efficient and accurate for comprehending the geological features of a particular site. Using remote sensing technology enables acquiring a wide range of data over extensive geographical regions.

Author contributions: Conceptualization, field investigation, data curation, methodology, software, analyzed results, writing—original draft, writing—review and editing, BAEH, AMY, TMM and AHES. All authors have read and agreed to the published version of the manuscript.

Conflict of interest: The authors declare no conflict of interest.

References

1. Peyghambari S, Zhang Y. Hyperspectral remote sensing in lithological mapping, mineral exploration, and environmental geology: an updated review. *Journal of Applied Remote Sensing*. 2021; 15(03). doi: 10.1117/1.jrs.15.031501
2. EL-Omairi MA, El Garouani A. A review on advancements in lithological mapping utilizing machine learning algorithms and remote sensing data. *Heliyon*. 2023; 9(9): e20168. doi: 10.1016/j.heliyon.2023.e20168
3. Othman A, Gloaguen R. Improving Lithological Mapping by SVM Classification of Spectral and Morphological Features: The Discovery of a New Chromite Body in the Mawat Ophiolite Complex (Kurdistan, NE Iraq). *Remote Sensing*. 2014; 6(8): 6867-6896. doi: 10.3390/rs6086867
4. Elaaraj A, Lhachmi A, Tabyaoui H, et al. Remote Sensing Data for Geological Mapping in the Saka Region in Northeast Morocco: An Integrated Approach. *Sustainability*. 2022; 14(22): 15349. doi: 10.3390/su142215349
5. El Fels AEA, El Ghorfi M. Using remote sensing data for geological mapping in semi-arid environment: a machine learning approach. *Earth Science Informatics*. 2022; 15(1): 485-496. doi: 10.1007/s12145-021-00744-w
6. Wang S, Huang X, Han W, et al. Lithological mapping of geological remote sensing via adversarial semi-supervised segmentation network. *International Journal of Applied Earth Observation and Geoinformation*. 2023; 125: 103536. doi: 10.1016/j.jag.2023.103536
7. Saadi NM, Watanabe K. Assessing image processing techniques for geological mapping: a case study in Eljufra, Libya. *Geocarto International*. 2009; 24(3): 241-253. doi: 10.1080/10106040802556199
8. Zhou G, Chen W, Qin X, et al. Lithological Unit Classification Based on Geological Knowledge-Guided Deep Learning Framework for Optical Stereo Mapping Satellite Imagery. *IEEE Transactions on Geoscience and Remote Sensing*. 2023; 61: 1-16. doi: 10.1109/tgrs.2023.3327774
9. Rajan Girija R, Mayappan S. Mapping of mineral resources and lithological units: a review of remote sensing techniques. *International Journal of Image and Data Fusion*. 2019; 10(2): 79-106. doi: 10.1080/19479832.2019.1589585
10. Chen Y, Wang Y, Zhang F, et al. Remote Sensing for Lithology Mapping in Vegetation-Covered Regions: Methods, Challenges, and Opportunities. *Minerals*. 2023; 13(9): 1153. doi: 10.3390/min13091153
11. Chen W, Li X, Qin X, et al. Remote Sensing Intelligent Interpretation for Geology. Springer Nature Singapore; 2024. doi: 10.1007/978-981-99-8997-3
12. Capello MA, Caslin E, Stewart I, et al. Creating a Geosciences Sustainability Atlas. Second International Meeting for Applied Geoscience & Energy. Published online August 15, 2022. doi: 10.1190/image2022-3751818.1
13. Gill JC, Smith M. Geosciences and the Sustainable Development Goals. Springer; 2021.
14. Brandolini P, Del Monte M, Faccini F, et al. Geomorphological mapping in urban areas. *Journal of Maps*. 2021; 17(4): 1-5. doi: 10.1080/17445647.2021.1952671
15. Said R. The Geological evolution of the River Nile. In: Wendorf F, Maks AF (editors). *Problems in Prehistory of Northern Africa and the Levant*. Southern Methodist University Press; 1975. pp. 1-44.
16. Issawi B, McCauley JF. The Cenozoic Rivers of Egypt: The Nile Problem. In: Freidman R, Adams B (editors). *The Followers of Horus*. Oxford Press; 1992.
17. Omer AA. Geological, mineralogical and geochemical studies on the Neogene and Quaternary Nile basin deposits, Qena-Assiut stretch, Egypt [PhD thesis]. South Valley University; 1996.

18. Mahran TM, El-Haddad AA. Facies and depositional environments of upper Pliocene- Pleistocene Nile sediments around Sohag area, Nile valley, Egypt. *Jornal of Saharian studies*. 1992; 1(2): 11-40.
19. Said R. *The River Nile: Geology, hydrology and utilization*. Pergamon Press; 1993.
20. Mahran T, Hassan AM. Controls on Late Miocene to Early Quaternary continental sedimentation during the development of the Sohag basin, Nile Valley, Egypt. *Journal of African Earth Sciences*. 2023; 199: 104829. doi: 10.1016/j.jafrearsci.2023.104829
21. Said R. Proposed classification of the Quaternary of Egypt. *Journal of African Earth Sciences*. 1983; 1(1): 41-45. doi: 10.1016/0899-5362(83)90030-1
22. Reddy GPO, Singh SK. *Geospatial Technologies in Land Resources Mapping, Monitoring and Management*. Springer International Publishing; 2018. doi: 10.1007/978-3-319-78711-4
23. Nemmour-Zekiri D, Oulebsir F. Application of remote sensing techniques in lithologic mapping of Djanet Region, Eastern Hoggar Shield, Algeria. *Arabian Journal of Geosciences*. 2020; 13(14). doi: 10.1007/s12517-020-05648-5
24. Ghrefat H, Kahal AY, Abdelrahman K, et al. Utilization of multispectral landsat-8 remote sensing data for lithological mapping of southwestern Saudi Arabia. *Journal of King Saud University - Science*. 2021; 33(4): 101414. doi: 10.1016/j.jksus.2021.101414
25. Issawi B. Archean-Phanerozoic birth and the development of the Egyptian Land. In *1st International Conference on the Geology of the Tethys*. 2005; 2: 380-380.
26. Issawi B, El-Hinnawi M, Francis M, et al. *The Phanerozoic geology of Egypt—a geodynamic approach*. The Egyptian Geological Survey Press; 1999.
27. Mahran TM, El-Shater A, Youssef AM, et al. Facies analysis and tectonic-climatic controls of the development of Pre-Eonile and Eonile sediments of the Egyptian Nile west of Sohag. In: *The 7th International Conference on the Geology of Africa*; 2013; Assiut, Egypt.
28. Said R. *The geological evolution of the river Nile*. Springer New York; 1981. doi: 10.1007/978-1-4612-5841-4
29. Capuzzo N, Wetzel A. Facies and basin architecture of the Late Carboniferous Salvan-Dorénaz continental basin (Western Alps, Switzerland/France). *Sedimentology*. 2004; 51(4): 675-697. doi: 10.1111/j.1365-3091.2004.00642.x
30. Sharama M, Sharma SM, Shuklam KU, et al. Sandstone body architecture and stratigraphic trend in the Middle Siwalik succession of the Jumma area, India. *Journal of Asian Earth Sciences*. 2022; 20(7): 817-828. doi: 10.1016/S1367-9120(01)00056-6
31. Miall AD. *The geology of fluvial deposits: sedimentary facies, basin analysis and petroleum geology*. Springer-Verlag; 1996.
32. Miall AD. Architectural elements and bounding surfaces in fluvial deposits: anatomy of the Kayenta formation (lower Jurassic). *Southwest Colorado Original Research Article Sedimentary Geology*. 1985; 55(3-4): 233-240,247-262. doi: 10.1016/0037-0738(88)90133-9
33. Lee S, Chough S. Changes in sedimentary facies and strata patterns along the strike-slip margin, northeastern Jinan Basin (Cretaceous), southwest Korea, implications for differential subsidence. *Sedimentary Geology*. 1999; 128: 81-102.
34. Akkad S, Dardir AA. *Geology of the Red Sea coast between Ras Ghagara and Mersa Alam, Egypt*. Geological survey. 1966; 35-67.
35. Mahran T. Cyclicity in Nakheil Formation (Oligocene), west of Quseir, Red Sea Egypt. *Egypt. Journal Geology*. 1997; 41(2A): 309-346.
36. Goudie AS. The drainage of Africa since the Cretaceous. *Geomorphology*. 2005; 67(3-4): 437-456. doi: 10.1016/j.geomorph.2004.11.008
37. Issawi B, Osman R. Egypt during the Cenozoic: geological history of the Nile river. *Bull Tethys Geological Society Cairo*. 2008; 3: 43-62.
38. Youssef AM, Abdel Moneim AA, Abu El-Maged SA. Flood hazard assessment and its associated problems using geographic information systems. Available online: https://www.researchgate.net/publication/259236978_Flood_hazard_assessment_and_its_associated_problems_using_geographic_information_systems_Sohag_Governorate_Egypt (accessed on 6 January 2024).